



# Reversible and irreversible gas–particle partitioning of dicarbonyl compounds observed in the real atmosphere

Jingcheng Hu, Zhongming Chen, Xuan Qin, and Ping Dong

State Key Laboratory of Environmental Simulation and Pollution Control, College of Environmental Sciences and Engineering, Peking University, Beijing, 100871, China

**Correspondence:** Zhongming Chen (zmchen@pku.edu.cn)

Received: 30 January 2022 – Discussion started: 9 February 2022

Revised: 9 May 2022 – Accepted: 11 May 2022 – Published: 31 May 2022

**Abstract.** Glyoxal and methylglyoxal are vital carbonyl compounds in the atmosphere and play substantial roles in radical cycling and ozone formation. The partitioning process of glyoxal and methylglyoxal between the gas and particle phases via reversible and irreversible pathways could efficiently contribute to secondary organic aerosol (SOA) formation. However, the relative importance of two partitioning pathways still remains elusive, especially in the real atmosphere. In this study, we launched five field observations in different seasons and simultaneously measured glyoxal and methylglyoxal in the gas and particle phases. The field-measured gas–particle partitioning coefficients were 5–7 magnitudes higher than the theoretical ones, indicating the significant roles of reversible and irreversible pathways in the partitioning process. The particulate concentration of dicarbonyls and product distribution via the two pathways were further investigated using a box model coupled with the corresponding kinetic mechanisms. We recommended the irreversible reactive uptake coefficient  $\gamma$  for glyoxal and methylglyoxal in different seasons in the real atmosphere, and the average value of  $8.0 \times 10^{-3}$  for glyoxal and  $2.0 \times 10^{-3}$  for methylglyoxal best represented the loss of gaseous dicarbonyls by irreversible gas–particle partitioning processes. Compared to the reversible pathways, the irreversible pathways played a dominant role, with a proportion of more than 90 % in the gas–particle partitioning process in the real atmosphere, and the proportion was significantly influenced by relative humidity and inorganic components in aerosols. However, the reversible pathways were also substantial, especially in winter, with a proportion of more than 10 %. The partitioning processes of dicarbonyls in reversible and irreversible pathways jointly contributed to more than 25 % of SOA formation in the real atmosphere. To our knowledge, this study is the first to systemically examine both reversible and irreversible pathways in the ambient atmosphere, strives to narrow the gap between model simulations and field-measured gas–particle partitioning coefficients, and reveals the importance of gas–particle processes for dicarbonyls in SOA formation.

## 1 Introduction

Glyoxal and methylglyoxal, the simplest  $\alpha$ -dicarbonyls, are recognized as being of great importance in atmospheric chemistry due to their unique physico-chemical properties. The  $\alpha$ -dicarbonyl functionality leads to higher water solubility and reactivity of dicarbonyls than expected as the  $\alpha$ -dicarbonyl functionality is hydrophilic and contributes to hydrate formation. The hydrate form of carbonyls is less volatile and more water-soluble than the unhydrated form (Lim et al., 2013) owing to the strong effect of the two hy-

drogen bonding groups in the hydrated form (Elrod et al., 2021). Moreover, hydrates can easily participate in continuous radical reactions with higher reactivity by H abstraction to form higher-molecular-weight oligomers (Michailoudi et al., 2021). The traditional opinion is that methylglyoxal is less reactive compared to glyoxal due to its unreactive methyl substitution, while a very recent study noted that methylglyoxal could be more reactive under an atmospheric-relevant concentration (Li et al., 2021). Overall, both of them play crucial roles in radiation balance, air quality, brown carbon

formation, and secondary organic aerosol (SOA) formation (Laskin et al., 2015; Qiu et al., 2020). Moreover, as major carcinogenic and genotoxic compounds, dicarbonyls can cause serious damage to human health. They have relatively limited primary sources, except for biomass burning and biofuel combustion (Zarzana et al., 2017, 2018), compared to secondary formation that occurs with photo-oxidation of both biogenic volatile organic compounds (VOCs), such as isoprene, and anthropogenic VOCs, such as aromatic hydrocarbons (Lv et al., 2019). Considering the atmospheric sink, glyoxal and methylglyoxal can be lost in the gas phase by self-photolysis, oxidation by active radicals (such as OH radicals, NO<sub>3</sub> radicals), and wet/dry deposition; however, there is still a missing sink for the two dicarbonyls (Volkamer et al., 2007), which is the gas–particle partitioning process that will be fully discussed in this study.

Gas–particle partitioning was recently found to be the most important removal pathway for both glyoxal and methylglyoxal, especially in regions like Beijing with high particulate matter (PM) pollution that provides sufficient aerosol surface area. Although they have relatively high vapour pressure, glyoxal and methylglyoxal can efficiently partition into the particle phase due to their  $\alpha$ -dicarbonyl functionality. The surface-adsorbed dicarbonyls could alter the properties of the particle's surfaces, and the organic surface films could act as a kinetic barrier to gas–aerosol mass transport and thereby influence particle equilibration and water/gas uptake (Donaldson and Vaida, 2006). Upon physical adsorption, besides desorption or reaction at the surface, dicarbonyls could undergo solvation and incorporation into the bulk liquid, and then they could go through diffusion and chemical reactions in the bulk phase. The product may return onto surfaces and into the gas phase or stay in the bulk phase (Davidovits et al., 2006). Moreover, chemical reactions occurring at the surface or in the bulk phase could in turn accelerate the physical adsorption and greatly contribute to the formation and growth of atmospheric particulate matter. While it is difficult to distinguish the surface reactions and bulk reactions in field observations, we regard both of them as particle-phase reactions in this study. The chemical reactions occurring in the gas–particle partitioning processes can be divided into reversible pathways, including reversible hydration and self-oligomerization, and irreversible pathways, which can be driven by oxidative compounds. These processes can also efficiently explain observed aerosol properties – including relatively high oxygenation levels, compositions such as organic acids and oligomers, and higher light absorption – that cannot be explained by traditional absorptive models of gas–particle partitioning (Pankow, 1994; Pankow and James, 1994; Odum et al., 1996).

Many laboratory and model studies have made a great effort to investigate the reversible and irreversible pathways of dicarbonyls to further understand their gas–particle partitioning mechanisms and reveal their contribution to SOA formation. Fu et al. (2008) found that the modelled SOA concentra-

tions were largely increased when accounting for irreversible uptake of dicarbonyls in the GEOS-Chem model. Considering the surface-controlled reactive uptake of dicarbonyls into the Community Multiscale Air Quality (CMAQ) model, the aerosol uptake of dicarbonyls accounted for more than 45 % of total SOA in the eastern US (Ying et al., 2015); similarly, the contribution of glyoxal and methylglyoxal to SOA formation in China was 14 % to 25 % and 23 % to 28 %, respectively (Hu et al., 2017). Although reversible and irreversible pathways of dicarbonyls have been separately investigated in previous studies, solely incorporating just one pathway into models could lead to a large discrepancy between model results and observational data, highlighting the importance of comprehensively considering both reversible and irreversible pathways when quantifying the gas–particle partitioning process of dicarbonyls (Li et al., 2014; Hu et al., 2017; Ling et al., 2020).

Despite increasing interest in dicarbonyls and their gas–particle partitioning processes, the detailed chemical mechanisms of two partitioning pathways remain poorly understood. First, previous studies have exposed seed particles to high concentration levels of dicarbonyl vapours, from hundreds of parts per billion to parts per million levels, or used bulk samples; thus, their applicability to the real atmosphere requires further validation. Second, prior studies always used one constant coefficient to present all heterogeneous processes occurring on the aerosol, which neglects the influencing factors in the real atmospheric partitioning processes. Further studies have shown that the two pathways in the gas–particle partitioning process for glyoxal and methylglyoxal are rather complex, and their relative contribution to the partitioning process can be influenced by many factors such as relative humidity (Curry et al., 2018; Shen et al., 2018), particle acidity (Liggio et al., 2005b; Shi et al., 2020), and particle organic/inorganic components (Kampf et al., 2013). However, there persist controversies in the specific partitioning mechanisms of glyoxal and methylglyoxal, especially conflicting views on their role in SOA formation, which urgently warrant further investigation.

In this study, five field observations were launched over urban Beijing in four seasons, and glyoxal and methylglyoxal in the gas and particle phases were simultaneously measured. Beijing, as the political centre of China, is the most prosperous city with numerous key environmental issues. Chen et al. (2021) found that the average concentration of dicarbonyls in Beijing is lowest among the key regions that have relatively higher PM<sub>2.5</sub> concentrations, indicating there is a more efficient partitioning process of dicarbonyls. Thus, it is more environmentally significant to discuss the gas–particle partitioning processes in urban Beijing. These processes are divided into reversible pathways and irreversible pathways, which are based on the reversibility of the chemical reaction of dicarbonyls occurring in the condensed phase (Galloway et al., 2009; Ervens and Volkamer, 2010; Kampf et al., 2013; Ling et al., 2020). On the basis of field-measured data,

we could estimate the product distribution, main influencing factors, and relative importance of the two gas–particle partitioning pathways for glyoxal and methylglyoxal in the real atmosphere.

## 2 Materials and method

### 2.1 Field sampling

We performed field observations on the roof of a six-story teaching building (26 m above the ground) on the Peking University campus (39.992° N, 116.304° E) in northwest urban Beijing. The field observations in this study were launched during four different seasons from 2019 to 2021.

Gaseous carbonyls were collected by adsorption reactions in a 2,4-dinitrophenylhydrazine (DNPH) cartridge (Sep-Pak; Waters Corporation). The air samples were first passed through an ozone scrubber (Sep-Pak; Waters Corporation) to eliminate interference by ozone and then trapped in the DNPH cartridge. To prevent deliquescence of the potassium iodide in the ozone scrubber, the air samples were mixed with ultrapure nitrogen before being pumped into the sampling tubing. Air samples were continuously collected every 3 h in daytime and 9 h in nighttime. The total flow rate was 0.8 L min<sup>-1</sup>.

Particulate carbonyls were collected by a four-channel ambient particle sampler (TH-16A, Wuhan Tianhong) with a Teflon filter and quartz filters (47 mm, Whatman). The Teflon filter was used to measure the mass concentration of collected PM<sub>2.5</sub> and water-soluble inorganic compounds (Na<sup>+</sup>, NH<sub>4</sub><sup>+</sup>, K<sup>+</sup>, Mg<sup>2+</sup>, Ca<sup>2+</sup>, Cl<sup>-</sup>, NO<sub>3</sub><sup>-</sup>, and SO<sub>4</sub><sup>2-</sup>). The quartz filters were used for carbonyl analysis. The flow rate was set at 16.7 L min<sup>-1</sup>, and particle samples were continuously collected every 12 h daily. Detailed information about field sampling and analysis was provided in previous studies (Rao et al., 2016; Qian et al., 2019). To estimate the positive artefacts by adsorption of gas-phase dicarbonyls onto the filter (Hart and Pankow, 1994; Mader and Pankow, 2001; Liggio, 2004; Odabasi and Seyfioglu, 2005), throughout our previous field observations, we placed a backup quartz filter after the particle sampling quartz filter using an independent filter holder. The sampling filters would collect the particles and adsorbed gaseous dicarbonyls, while the backup filter would only collect gaseous dicarbonyls. The ratio of measured dicarbonyls in the second filter to that in the first was lower than 20 %, which was equal to the previous study (Shen et al., 2018). The particulate concentrations of dicarbonyls used in this study were already corrected by the possible adsorption artefacts.

The meteorological station was co-located at our sampling site and provided meteorological parameters. Common trace gases, such as NO/NO<sub>2</sub>, SO<sub>2</sub>, CO, and O<sub>3</sub>, were detected online by Thermo 42i, 43i, 48i, and 49i analysers, respectively. A TEOM 1400A analyser was applied to measure the mass concentrations of PM<sub>2.5</sub> and PM<sub>10</sub>, the results of which were

consistent with the PM<sub>2.5</sub> weighing results (Fig. S1 in the Supplement). The time resolution for all of the above data was 1 min. Detailed information about these five observations is shown in Table S1 in the Supplement.

### 2.2 Sample extraction and analysis

The gaseous carbonyl samples were eluted with acetonitrile (HPLC/GC-MS – high-performance liquid chromatography and gas chromatography–mass spectroscopy – grade) at a flow rate of less than 3 mL min<sup>-1</sup> (higher flow rates can result in reduced recovery), and the particulate carbonyl samples on the quartz filter were eluted with acidic DNPH solutions in the flask and then were shaken for 3 h at 4 °C with a rotation rate of 180 rpm in an oscillator (Shanghai Zhicheng ZWY 103D). The derived solutions were placed in darkness for 12–24 h to ensure complete derivatization, and then they were analysed by HPLC ultraviolet (HPLC-UV) for separation and detection. Carbonyls were separated effectively from each other (Fig. S2 in the Supplement) in this method. They were calibrated using a mixing standard solution with a concentration range of 0.1–10 μM, and the linearity was indicated by a correlation of determination (*r*<sup>2</sup>) of at least 0.999. The detailed analysis method was presented in the previous study (Wang et al., 2009).

The Teflon samples were also extracted by deionized water using an ultrasonic bath for 30 min at room temperature. The extracted solutions were analysed by ion chromatography (IC Integriion and Dionex ICS-2000, USA) to measure the water-soluble inorganic compounds (Na<sup>+</sup>, NH<sub>4</sub><sup>+</sup>, K<sup>+</sup>, Mg<sup>2+</sup>, Ca<sup>2+</sup>, Cl<sup>-</sup>, NO<sub>3</sub><sup>-</sup>, and SO<sub>4</sub><sup>2-</sup>) and low-molecular-weight organic acids (formate, acetate, and oxalate) in aerosols.

### 2.3 Quality assurance and quality control

As carbonyl compounds are ubiquitous in environmental media, the following measurements were conducted during the sample collection, pretreatment, and analysis to ensure the accuracy of results: (1) before sampling, flow calibration and airtightness tests of sampling devices were conducted, and flow differences were less than 10 %; (2) after sampling, the gas-phase samples were resealed by their end cap and plug and stored in the provided pouch in a cool environment (< 4 °C); the particle-phase samples were stored in the sealed boxes wrapped by pre-baked aluminium foils in a freezing environment (< -18 °C), and both gas-phase and particle-phase samples were extracted and analysed within a week; (3) the extraction processes were conducted in fume hood with glassware, which was rinsed with acetonitrile at least three times; and (4) a calibration run was performed each day to determine the response factor of the detector and recalibration was performed if the relative deviation of the response factor was beyond 5 %.

Blank samples were collected every 3 d and then were stored and extracted by the same procedure as that for am-

bient samples. The blank gas-phase samples were collected by placing blank DNPH cartridges near the gas inlet for the same duration without artificial pumping, and the blank particle-phase samples were collected by placing a blank quartz filter on the PM<sub>2.5</sub> inlet with a flow rate of 0 L min<sup>-1</sup>. All data used in this study were calibrated by blanks.

The limit of detection (LOD) of two methods was 50 pptv (parts per trillion by volume) for gaseous carbonyls and 1 ng m<sup>-3</sup> for particulate carbonyls, which is similar to the previous literature (Shen et al., 2018). Sample amount to limit of detection ratios were significantly higher than 1.0 for both gas- and particle-phase samples, indicating that the sensitivity of the methods was sufficient to analyse the samples.

Additional field samplings were launched to estimate the sampling efficiency during the collection. Two blank DNPH cartridges were connected in tandem to assess the sampling efficiency of gas-phase carbonyls. The sampling efficiency of the cartridges was the ratios of dicarbonyl concentrations in the first cartridge to the total concentrations in the two cartridges, and the results were more than 95 % for both glyoxal and methylglyoxal. Similarly, a backup Teflon filter was placed after the particle sampling Teflon filter using an independent filter holder to estimate the particle collection efficiency. Both Teflon filters were weighed by a semi-micro balance (Sartorius, Germany) to obtain the mass concentration of collected particles. The mass concentrations of particles collected on the backup filter were close to zero, indicating that the sampling efficiency of particle was more than 99 %.

Moreover, recovery tests were also conducted using two methods – adding standard solution and repeated extraction. We added the standard solution at three spiked levels of 0.025, 0.25, and 2.5 µg (namely 50 µL of 0.5, 5, and 50 µg mL<sup>-1</sup> analytical standards) into blank DNPH cartridges and on a blank quartz filter to determine the carbonyl lost during the extraction and derivation. Then the cartridges and filters were extracted in the same way as the ambient samples. Each group was set with five parallel cartridges/filters. The recoveries were ranged from 88 % to 96 % for the gas-phase method and ranged from 85 % to 96 % for the particle-phase method. Moreover, we also estimated the recovery efficiencies by repeated extraction, and the recoveries were the ratios of dicarbonyl concentrations in the first extraction to the total concentrations in the two extractions. The results ranged from 92.8 % to 99.9 % for the gas-phase method and ranged from 90 % to 99.9 % for the particle-phase method.

#### 2.4 Estimation of effective partitioning coefficient

To estimate the effective partitioning process of gas-phase carbonyls to the particle phase, we could use Pankow's absorptive partitioning theory for the gas–organic phase (Eqs. 1 and 2) (Odum et al., 1996) and Henry's law for the gas–liquid

phase (Eq. 3):

$$K_p^f = \frac{C_p}{C_g \times \text{TSP}}, \quad (1)$$

$$K_p^t = \frac{RT f_{\text{om}}}{10^6 \text{MW}_{\text{OM}} \zeta p_L^0}, \quad (2)$$

$$\text{eff}K_H = 10^3 \frac{c_p}{c_g \times M \times \text{ALWC} / \rho_{\text{water}}}. \quad (3)$$

In Eq. (1),  $K_p^f$  (m<sup>3</sup> µg<sup>-1</sup>) is the field-measured gas–particle partitioning coefficient;  $C_p$  (µg m<sup>-3</sup>) is the concentration of dicarbonyls in the particle phase, which is derived from the analysis of extracts, including monomers and their reversibly formed products (the product distribution is discussed in Sect. 3.2);  $C_g$  (µg m<sup>-3</sup>) is the concentration of dicarbonyls in the gas phase; and TSP (µg m<sup>-3</sup>) is the mass concentration of suspended particles (mass concentrations of PM<sub>2.5</sub> were used in this study). In Eq. (2),  $K_p^t$  (m<sup>3</sup> µg<sup>-1</sup>) is the theoretical gas–particle partitioning coefficients determined by Pankow's absorptive model,  $f_{\text{om}}$  is the absorbing fraction of total particulate mass,  $\text{MW}_{\text{OM}}$  (g mol<sup>-1</sup>) is the mean molecular weight of the organic phase, and  $\zeta$  is the activity coefficient of target compounds. In the estimation of  $K_p^t$  in this study,  $f_{\text{om}}$  and  $\zeta$  are unity and  $\text{MW}_{\text{OM}} = 200$  g mol<sup>-1</sup>, as used in previous studies (Healy et al., 2008; Williams et al., 2010; Xie et al., 2014; Shen et al., 2018), and  $p_L^0$  (Pa) is the supercooled vapour pressure of compounds as a pure liquid at temperature  $T$ , which is calculated by the extended aerosol inorganic model (E-AIM; [http://www.aim.env.uea.ac.uk/aim/ddbst/pcalc\\_main.php](http://www.aim.env.uea.ac.uk/aim/ddbst/pcalc_main.php), last access: 23 May 2021) (Clegg et al., 1998). The possible uncertainty in  $K_p^t$  calculation is fully discussed in the Supplement. In Eq. (3),  $\text{eff}K_H$  (Matm<sup>-1</sup>) is the field-derived effective Henry's law coefficient;  $c_p$  (µg m<sup>-3</sup>) and  $c_g$  (atm) are particle- and gas-phase concentrations of carbonyls, respectively; and ALWC (µg m<sup>-3</sup>) is the aerosol liquid water content calculated by the thermodynamic model ISORROPIA-II (forward model, metastable state), the results of which are comparable to the actual measured contents confirmed by previous studies (Guo et al., 2015).

The irreversible reactive uptake coefficient  $\gamma$  could efficiently describe the irreversible pathways of the gas–particle partitioning process of dicarbonyls driven by OH radicals. We could estimate the reactive uptake coefficient  $\gamma$  based on the effective Henry's constant via theory calculation (Hanson et al., 1994; Curry et al., 2018) and then calculate the effective uptake rate,  $k_{\text{eff,uptake}}$ , following Eqs. (4)–(7):

$$\frac{1}{\gamma} = \frac{1}{\alpha} + \frac{v}{4RT \text{eff}K_H \sqrt{k^1 D_{\text{aq}}}} \times \frac{1}{[\coth q - 1/q]}, \quad (4)$$

$$v = \sqrt{\frac{8RT}{\pi M_X}}, \quad (5)$$

$$q = \frac{R_p}{l} = \frac{R_p}{\sqrt{\frac{D_{\text{aq}}}{k^1}}}, \quad (6)$$

$$k_{\text{eff,uptake}} = \frac{1}{4}v \times \gamma \times A_{\text{surf}}, \quad (7)$$

where  $\gamma$  is the dimensionless uptake coefficient,  $v$  ( $\text{m s}^{-1}$ ) is the gas-phase thermal velocity of glyoxal/methylglyoxal,  $D_{\text{aq}}$  ( $\text{m}^2 \text{s}^{-1}$ ) is the diffusion coefficient in the liquid phase,  $\alpha$  is dimensionless mass accommodation coefficient,  $\text{eff}K_{\text{H}}$  ( $\text{Matm}^{-1}$ ) is the effective Henry's law constant calculated by field-measured data in Table 2,  $R$  is the universal gas constant,  $k^1$  ( $\text{s}^{-1}$ ) is the first-order aqueous loss rate,  $M_X$  ( $\text{kg mol}^{-1}$ ) is the average molar mass of gas-phase dicarbonyls,  $q$  is the parameter for measuring in-particle diffusion limitations,  $R_p$  (m) is the particle radius,  $l$  (m) is the diffusion reactive length,  $k_{\text{eff,uptake}}$  ( $\text{s}^{-1}$ ) is the effective uptake rate, and  $A_{\text{surf}}$  ( $\text{m}^2 \text{m}^{-3}$ ) is the aerosol surface area density. This formulation is based on the effective Henry's law constant under high relative humidity (RH) conditions (RH > 40 %). Moreover, the formulation describes the reactive uptake due to irreversible multiple-phase loss processes in the presence of OH. The uncertainty in the  $\gamma$  calculation is mainly attributed to the uncertainty in OH concentration, which was  $3 \times 10^{-12}$  M on average and varied from  $5.5 \times 10^{-14}$  to  $8 \times 10^{-12}$  M (Herrmann et al., 2010).

### 3 Result and discussion

#### 3.1 Observation results and partitioning coefficients calculation

##### 3.1.1 Dicarbonyls in the gas and particle phases

We launched five field observations in different seasons. Table S1 details the information about the field observations, including observation periods, sample volume, and meteorological parameters. In total, we collected 387 gas-phase samples and 130 particle-phase samples in four seasons. In these samples, carbonyls were simultaneously measured in both gas phase and particle phases. A total of 10 carbonyls were measured in the gas phase, including formaldehyde, acetaldehyde, acetone, propionaldehyde, methacrolein, butyraldehyde, methyl vinyl ketone, benzaldehyde, glyoxal, and methylglyoxal, and six carbonyls were measured in the particle phase, including formaldehyde, acetaldehyde, acetone, propionaldehyde, glyoxal, and methylglyoxal. In this study, we mainly discuss the gas–particle partitioning processes of glyoxal and methylglyoxal because of their significant roles in atmospheric chemistry.

Figure 1 and Table 1 show the temporal characteristics of and seasonal variation in glyoxal and methylglyoxal, respectively. Gaseous dicarbonyls showed obvious seasonal variation. Concentrations in summer ( $0.99 \pm 0.59$  ppbv) were gen-

erally much higher than in other seasons, followed by autumn and spring, and the concentrations in winter were the lowest. This seasonal variation could be partly attributed to the higher temperature and more intensive radiation in summer, which could greatly enhance the secondary formation of gaseous carbonyls via photochemical reactions. The diurnal variation in the dicarbonyls during summer support this interpretation of the data; gas-phase dicarbonyls exhibited obviously diurnal variations in summer, whereas this variation was irregular in other seasons (Fig. S3 in the Supplement). The concentration levels of gaseous dicarbonyl in summer rapidly increased after sunrise, remained relatively high during the daytime (12:00–14:00 LT), and then decreased at dusk. Although methylglyoxal has a shorter lifetime compared to glyoxal (glyoxal 2.9 h vs. methylglyoxal 1.6 h) (Fu et al., 2008), its gas-phase concentration levels were generally higher than those of glyoxal, consistent with previous studies (Rao et al., 2016; Mitsuishi et al., 2018; Qian et al., 2019) mainly due to the relatively larger production from isoprene and acetone for methylglyoxal.

The concentrations of particulate dicarbonyls were an order of magnitude smaller than the gaseous concentrations using the unit of nanogram per cubic metre of air ( $\text{ng m}^{-3}$  air). The average particulate glyoxal and methylglyoxal were 19.37 and 11.24  $\text{ng m}^{-3}$ , respectively, which were slightly higher than previously reported values (Zhu et al., 2018; Shen et al., 2018; Qian et al., 2019; Cui et al., 2021). Dicarbonyls measured in the particle phase also showed obvious seasonal variation. The particulate concentrations of the two dicarbonyls in winter ( $43.38 \pm 32.42$   $\text{ng m}^{-3}$  air) were 2–2.3 times higher than those in other seasons, suggesting that the dicarbonyls were more favoured in the particle phase in winter. Moreover, particulate dicarbonyls in different seasons exhibited the same diurnal variation (Fig. S3). The particulate concentrations of dicarbonyls in daytime were generally higher than those in nighttime, especially in winter.

##### 3.1.2 Gas–particle partitioning coefficient

Dicarbonyls could partition between gas and aerosol phases or the liquid phase, following Pankow's absorptive partitioning theory or Henry's law, respectively, as listed in Table 2. Both gas–particle partitioning coefficient ( $K_{\text{p}}^{\text{f}}$ ) and effective Henry's law coefficient ( $K_{\text{H}}^{\text{f}}$ ) were calculated on the basis of field-measured data and were in the range of  $10^{-4}$ – $10^{-2}$   $\text{m}^3 \mu\text{g}^{-1}$  and  $10^6$ – $10^8$   $\text{Matm}^{-1}$ , respectively. The partitioning coefficient values of the two dicarbonyls exhibited the same seasonal variation, as winter and spring > autumn > summer. A higher aerosol concentration accompanied by higher aerosol surface area concentration and lower relative humidity resulted in a higher partitioning coefficient in winter and spring, when heavy pollution and sandstorms always occurred. In the case of temperature variation varying from 265.53 to 310.75 K in different seasons, lower temperature promoted the gas-to-particle partitioning processes as  $K_{\text{p}}^{\text{f}}$

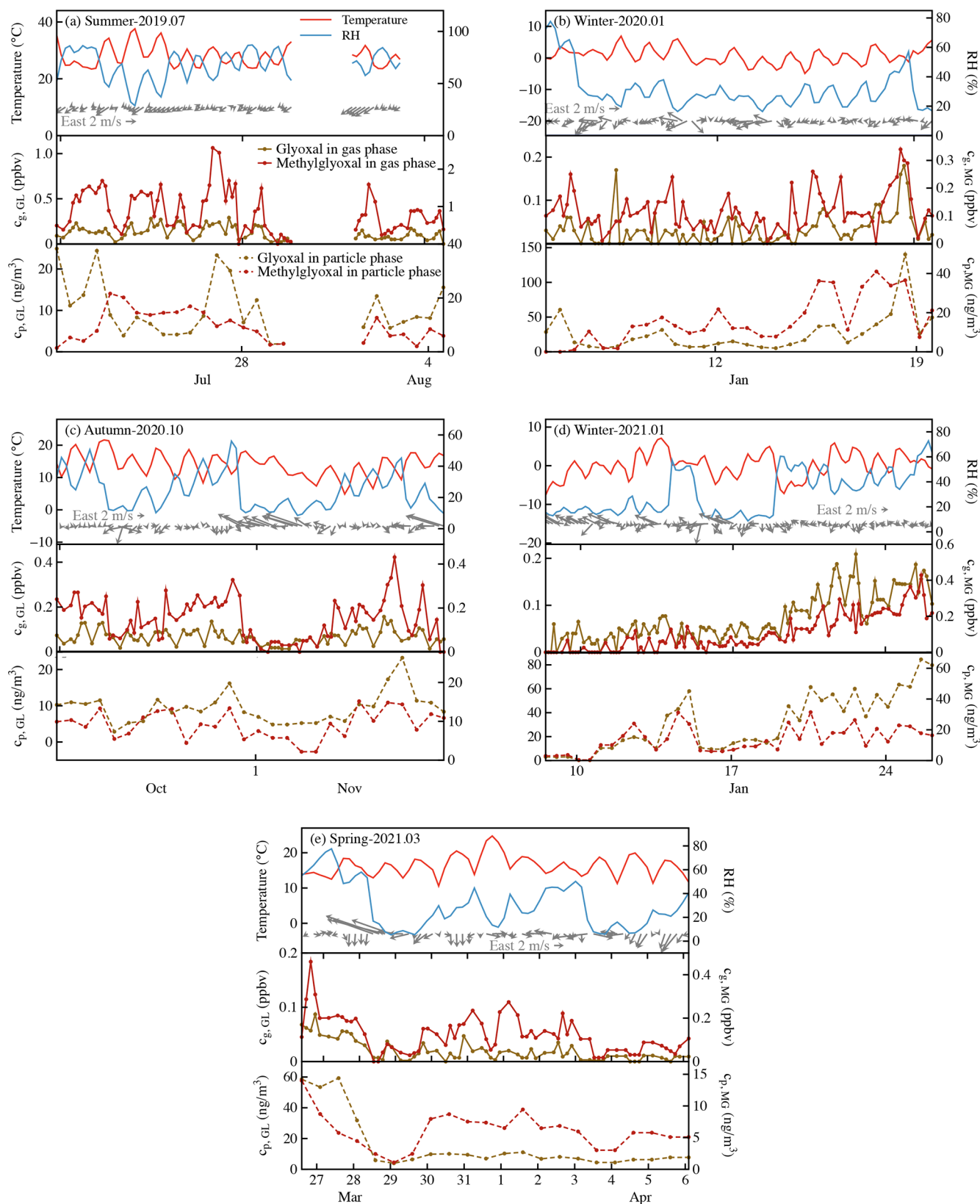


**Figure 1.** Time series of meteorological parameters and gas- and particle-phase glyoxal and methylglyoxal observed in different seasons: (a) summer, 20 July–4 August 2019; (b) winter, 5–19 January 2020; (c) autumn, 24 October–7 November 2020; (d) winter, 8–26 January 2021; and (e) spring, 26 March–6 April 2021.

**Table 1.** Statistical data for the  $\alpha$ -dicarbonyls in gas and particle phases in different seasons.

Season	Dates of the measurements (yyyy.mm.dd)	Gas phase (ppbv)		Particle phase (ng m <sup>-3</sup> )	
		Glyoxal	Methylglyoxal	Glyoxal	Methylglyoxal
Summer	2019.07.20–08.04	0.13 ± 0.07	0.87 ± 0.54	10.18 ± 6.63	9.50 ± 5.62
Spring	2021.03.26–04.06	0.02 ± 0.02	0.12 ± 0.08	15.24 ± 17.50	6.07 ± 2.79
Autumn	2020.10.24–11.07	0.07 ± 0.03	0.15 ± 0.09	9.33 ± 4.24	9.15 ± 3.62
Winter	2020.01.05–01.19, 2021.01.08–01.26	0.06 ± 0.05	0.11 ± 0.09	28.77 ± 25.33	14.61 ± 10.15

values for the dicarbonyls and temperature showed negative correlation with significant difference ( $p < 0.001$ ) (Fig. S4 in the Supplement). Moreover, The  $K_p^f$  and  $K_H^f$  values of glyoxal were always higher than those of methylglyoxal, implying the former was more likely to partition to the particle phase; this could be attributed to their different structures. Glyoxal were more soluble and reactive because of the adjacent electron-poor aldehydic carbons, whereas methylglyoxal was more stable due to the reduced electron-deficient ketone moiety (Kroll et al., 2005).

Both  $K_p^f$  and  $K_H^f$  values were relatively close to those found in previous field-measured studies (Shen et al., 2018; Qian et al., 2019; Cui et al., 2021). However, compared with the theoretical partitioning coefficient  $K_p^t$  calculated by Pankow's absorptive theory,  $K_p^f$  values were approximately 5–7 orders of magnitudes higher than the corresponding  $K_p^t$  values. Similarly,  $K_H^f$  values were approximately 2–5 orders of magnitudes higher than the theoretical Henry's law coefficient  $K_H^t$  calculated in pure water, which could be attributed to salting effects in wet aerosol (Fig. S5 in the Supplement).  $K_p^f$  and  $K_p^t$  values in this study were close to but slightly higher than the values published in previous literature (Table S2 in the Supplement), and the discrepancy between field-measured partitioning coefficients and the theoretical ones is fully discussed in the Supplement.

To narrow the large discrepancy between field-measured partitioning coefficients and theoretical ones, we needed to further investigate the mechanism and product distribution of chemical reactions occurring in the aerosols during the partitioning processes. The products of the reversible and irreversible pathways mostly have lower saturated vapour pressure, thus leading to higher partitioning coefficients compared to monomer dicarbonyls. Take glyoxal for example; the effective saturation vapour pressures of the product set in reversible pathways are  $\sim 10^{-5}$  Torr in the real atmosphere (Shen et al., 2018), and the products of the irreversible pathways had much lower vapour pressure values than those of reversible pathways; for example, the vapour pressure of oxalic acids and ammonium oxalates are  $\sim 10^{-5}$  Torr (Saxena and Hildemann, 1996) and  $5.18 \times 10^{-8}$  Torr (Lim et al., 2013), respectively, and those of glyoxal trimer dihydrates are  $\sim 10^{-11}$  Torr at 20 °C (Hilal et al., 1994), indicating the irreversible pathways make larger contributions to the under-

estimation of partitioning processes of dicarbonyls. The following sections further discuss the mechanism and product distribution of reversible and irreversible pathways to explain the partitioning process of dicarbonyls.

### 3.2 Reversible pathways

Gas–particle partitioning of dicarbonyls via reversible pathways mainly consists of hydration and self-oligomerization. Since glyoxal and methylglyoxal had high water solubility and reactivity, they could easily dissolve into aerosol liquid water and then form hydrates and oligomers. Hemiacetal/acetal formation (Loeffler et al., 2006) and aldol condensation (Haan et al., 2009) are the most thermodynamically favoured oligomer reactions for glyoxal hydrates and methylglyoxal hydrates, respectively. The proposed mechanism for the reversible formation of glyoxal and methylglyoxal in aerosols is shown in Fig. S6 in the Supplement. By adding excess derivatization agent (like 2,4-dinitrophenylhydrazine in this study), dicarbonyls, as well as their reversibly formed products, are efficiently transformed into dicarbonyl-bis-2,4-dinitrophenylhydrazine, which are quantified as monomers by means of analysis techniques (Kampf et al., 2013). Moreover, Healy et al. (2008) have confirmed that derivatization agent was found to efficiently dissolve a trimeric glyoxal standard and convert the resulting monomers to oxime derivatives, and oligomers could not be detected in the extracts of filter samples by GC-MS analysis, also indicating the use of excess derivatization agent could efficiently convert the hydrates and oligomers back to the monomeric species by removing dicarbonyl monomers from the extract as soon as they are formed. Both dissolved dicarbonyl monomers and reversibly formed products are efficiently transformed into carbonyl-bis-2,4-dinitrophenylhydrazine, which was quantified by means of HPLC-UV in this study. The concentrations of dissolved dicarbonyl monomers were estimated using Henry's law coefficients, which is used to determine the physical solubility of carbonyls (e.g.  $K_H = 5 \text{ M atm}^{-1}$  for glyoxal) (Schweitzer et al., 1998). The results were negligible compared to the concentrations of carbonyls in hydrate and oligomer forms. Thus, the concentrations of particle-phase dicarbonyl in reversible partitioning pathways were close to the measured concentration of carbonyls by HPLC-UV.

**Table 2.** Comparison of the field-measured partitioning coefficient  $K^f$  values for the dicarbonyls and their corresponding theoretical  $K^t$  values in different seasons.

Coefficients	Dicarbonyl	Season	$K^f$		$K^{t*}$	$K^f/K^t$
			Average	Range		
Gas–particle partitioning coefficients ( $\text{m}^3 \mu\text{g}^{-1}$ )	Glyoxal	Summer	$8.11 \times 10^{-4}$	$(1.25\text{--}58.6) \times 10^{-4}$	$3.27 \times 10^{-10}$	$2.48 \times 10^6$
		Autumn	$2.14 \times 10^{-3}$	$(2.61\text{--}224) \times 10^{-4}$	$6.27 \times 10^{-10}$	$3.41 \times 10^6$
		Spring	$1.43 \times 10^{-2}$	$(0.08\text{--}14.6) \times 10^{-2}$	$5.59 \times 10^{-10}$	$3.55 \times 10^7$
		Winter	$1.30 \times 10^{-2}$	$(0.067\text{--}44.2) \times 10^{-2}$	$1.27 \times 10^{-9}$	$1.02 \times 10^7$
	Methylglyoxal	Summer	$1.49 \times 10^{-4}$	$(0.833\text{--}169) \times 10^{-5}$	$7.10 \times 10^{-10}$	$2.10 \times 10^5$
		Autumn	$9.55 \times 10^{-4}$	$(0.65\text{--}86.9) \times 10^{-4}$	$1.35 \times 10^{-9}$	$7.07 \times 10^5$
		Spring	$1.06 \times 10^{-3}$	$(0.42\text{--}108) \times 10^{-4}$	$1.21 \times 10^{-9}$	$8.77 \times 10^5$
		Winter	$2.60 \times 10^{-3}$	$(0.34\text{--}410) \times 10^{-4}$	$2.72 \times 10^{-9}$	$9.93 \times 10^5$
Henry's law coefficients ( $\text{M atm}^{-1}$ )	Glyoxal	Summer	$1.96 \times 10^8$	$(1.71\text{--}167) \times 10^7$	$3.29 \times 10^5$	$6.11 \times 10^2$
		Autumn	$5.08 \times 10^8$	$(1.88\text{--}10.2) \times 10^8$	$1.14 \times 10^6$	$3.63 \times 10^3$
		Spring	$2.53 \times 10^9$	$(1.23\text{--}139) \times 10^8$	$9.03 \times 10^5$	$1.92 \times 10^4$
		Winter	$1.04 \times 10^9$	$(1.37\text{--}55.4) \times 10^8$	$4.15 \times 10^6$	$2.55 \times 10^3$
	Methylglyoxal	Summer	$4.92 \times 10^7$	$(1.70\text{--}363) \times 10^6$	$2.73 \times 10^3$	$1.88 \times 10^4$
		Autumn	$8.52 \times 10^7$	$(3.66\text{--}15.7) \times 10^7$	$9.50 \times 10^3$	$2.00 \times 10^5$
		Spring	$1.33 \times 10^8$	$(5.22\text{--}456) \times 10^6$	$7.49 \times 10^3$	$1.36 \times 10^5$
		Winter	$2.63 \times 10^8$	$(1.03\text{--}175) \times 10^7$	$3.44 \times 10^4$	$9.01 \times 10^4$

\* Theoretical gas–particle partitioning coefficients were calculated on the basis of Eq. (3), and theoretical Henry's law coefficients here referred to the Henry's law constant in pure water, which were calculated on the basis of Eqs. (S1) and (S2) in the Supplement (Ip et al., 2009; Sander, 2015).

As glyoxal and methylglyoxal have a similar trend under different conditions, we focused on the total concentration of the two dicarbonyls in the following discussion. As shown in Fig. 2a, the particulate concentration of dicarbonyls via a reversible pathway was strongly dependent on RH. It increased significantly when RH increased from  $< 10\%$  to  $60\%$  as dicarbonyls were more favourable to dissolve into hygroscopic aerosols during their growth (Mitsuishi et al., 2018; Xu et al., 2020). However, from  $60\%$  to  $80\%$  RH, it exhibited the opposite trend and decreased with increasing RH as higher water concentrations at elevated RH levels may dilute the monomer concentration in the particle phase and hinder oligomerization reactions (Healy et al., 2009), and the product distribution of the reversible formation could also explain this phenomenon well. The results exhibited a similar pattern to a previous study, in which the partitioning of glyoxal and methylglyoxal gradually increased as RH increased to  $40\%$ , peaked sharply around  $50\%$ , and subsequently decreased as RH increased towards  $80\%$  (Healy et al., 2009). Moreover, ionic strength could also influence the reversible partitioning process as it is closely related to aerosol liquid water and RH conditions. The presence of inorganic ions could catalyse and participate in oligomerization reactions via salting effects (Sareen et al., 2010; Mcneill, 2015). Whereas increasing viscosity of particles with increasing ionic strength could slow down all particle-phase reactions, the reversible nucleophilic addition of inorganic ions (e.g. sulfate ions) at car-

bonyl carbons deactivates the molecule for further oligomerization (Kampf et al., 2013).

To roughly estimate the product distribution of the reversible pathway in the real atmosphere, we simplified reaction mechanisms and calculated the product distribution on the basis of the kinetic mechanisms listed in Table S3 in the Supplement using a 0-D box model with a steady-state approach. Generally, more dicarbonyls existed in oligomer forms than in hydrate forms in the reversible formation. Moreover, their distribution exhibited obvious seasonal variations. Summer had the highest proportion of hydrate forms, while winter had the highest proportion of oligomer forms. Detailed information is shown in Table S4 in the Supplement. The seasonal variation could be attributed to the RH in different seasons – relatively high in summer and low in winter. As shown in Fig. 2b, the product distribution of the reversible formation has a strong dependence on RH. The proportion of dicarbonyls in hydrate forms increased with increasing RH and could reach more than  $75\%$  in high RH, while the proportion of dicarbonyls in oligomer forms exhibited the opposite trend. Hydrates play a dominant role in dilute solutions under high RH conditions with a relatively high aerosol liquid water concentration, which might hinder oligomer formation, and large quantities of oligomers, including dimers and trimers, would form until the aerosol liquid concentration became greater than  $1\text{ M}$  (Liggio et al., 2005b) when RH decreased. However, the product distribution here was simulated based on the bulk-phase mechanisms, and higher

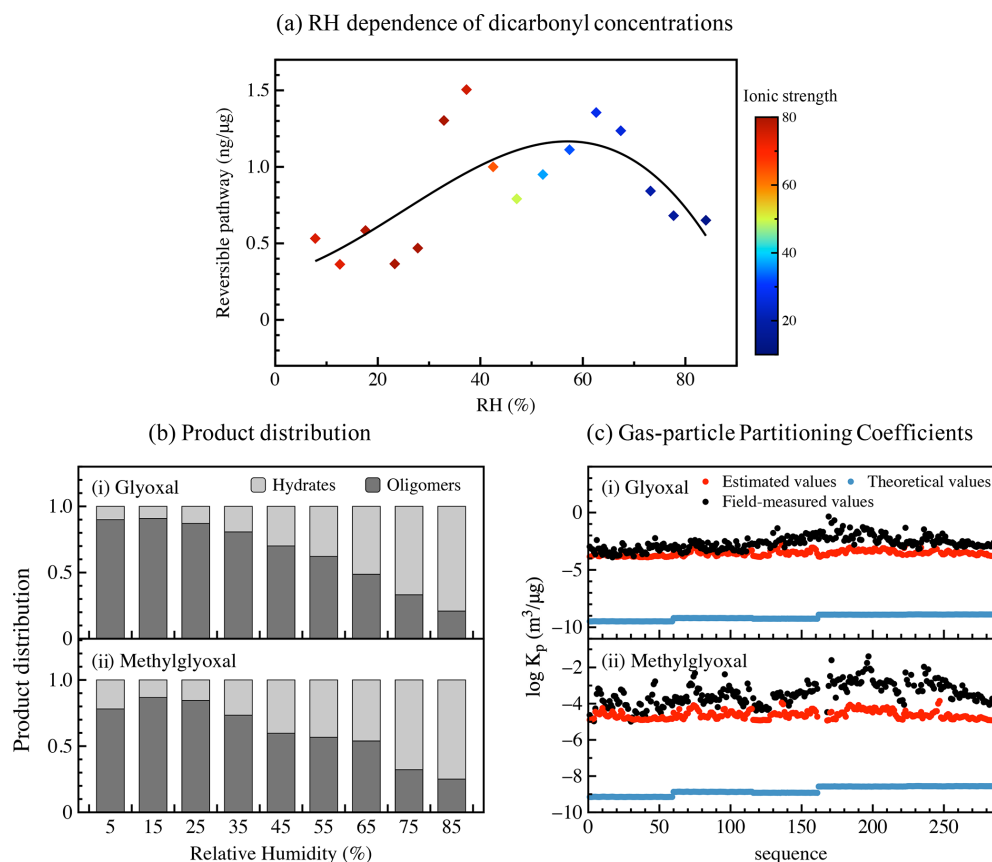


**Figure 2.** Gas–particle partitioning of dicarbonyls via reversible pathways. **(a)** The RH dependence of particulate concentrations of dicarbonyl via reversible pathways. **(b)** The product distribution for (i) glyoxal and (ii) methylglyoxal under different RH conditions. **(c)** The gas–particle partitioning coefficients for (i) glyoxal and (ii) methylglyoxal. The black, red, and blue circles refer to field-measured values, estimated values by the proposed mechanism, and theoretical values calculated by Pankow’s absorptive model, respectively.

ionic strength in aerosol phase would influence reaction equilibria and rate constants (Ervens and Volkamer, 2010; McNeill, 2015). The lack of quantitative reaction rate in aerosol phase could contribute more uncertainties to the simulation, whereas the RH dependence of product distribution and the order of magnitude of estimated  $K_p$  values were close to those in aerosol-phase, and the rough simulation could help us to understand the reversible partitioning pathways of dicarbonyls.

Combined with the vapour pressure of dominant products published in previous studies (Hastings et al., 2005; Axson et al., 2010), their gas–particle partitioning coefficient can be roughly estimated and can effectively fit the field-measured values, as shown in Fig. 2c. The estimated gas–particle partitioning coefficients in this study are 5 orders of magnitude higher than the theoretical ones but still 1–2 orders of magnitude lower than the field-measured coefficients, especially in winter. The difference between the estimated partitioning coefficients and the field-measured ones suggests that the current understanding of the equilibrium in reversible formations cannot reasonably explain the gas–particle partition-

ing processes of dicarbonyls. There still exist extra pathways of reversible formation. Cross-oligomerization of glyoxal and methylglyoxal is non-negligible and could form similar molecular structure products and contribute to SOA yield (Schwier et al., 2010). Esterification and amination of diols also occur in aerosol liquid water but are negligible compared to hydration and polymerization (Zhao et al., 2006). However, these reactions are not further discussed here. The hydrates and oligomers mentioned above are the dominant forms of glyoxal/methylglyoxal in the particle phase, while the higher molecular oligomers up to nonamer could also exist with a relatively smaller but still significant fraction at equilibrium. Although the reactions are thermodynamically reversible, upon evaporation of the aerosol liquid water, the oligomer formation is faster than the evaporation of dehydrated dicarbonyls, and the dicarbonyl evaporation is limited (Liggio et al., 2005b; Loeffler et al., 2006). This results in relatively stable oligomers and yields SOA. Moreover, other nucleophilic species may also form oligomers with glyoxal and methylglyoxal and effectively prevent their evaporation. Besides reversible pathways, higher carbon number prod-

ucts with lower volatility were mainly formed through irreversible pathways, such as radical reactions (e.g. OH radicals), which are fully discussed in the next section.

### 3.3 Irreversible pathways

#### 3.3.1 Irreversible pathways driven by hydroxyl radicals

Reactive uptake driven by hydroxyl radicals (OH) is the dominant process for glyoxal and methylglyoxal in their irreversible gas–particle partitioning pathways. Compared to other irreversible pathways, such as imidazole formation, glyoxal/methylglyoxal + OH chemistry occurs on much shorter timescales (Teich et al., 2016). The reaction is the initial step for most radical-based chemistry of glyoxal/methylglyoxal and has been proven to be an important source of SOA in both cloud/fog droplets and wet aerosols (Tan et al., 2012; Lim et al., 2013), producing low-volatility products such as organic acids, large multifunctional humic-like substances, and oligomers. The proposed mechanism for the irreversible pathway of glyoxal and methylglyoxal driven by hydroxyl radicals in aerosols is shown in Fig. S7 in the Supplement. The OH radicals in aerosol liquid water are mainly from the direct uptake of gas-phase OH radicals with a Henry's law constant of  $30 \text{ M atm}^{-1}$  (Faust and Allen, 1993), and Fenton reactions are closely related to hydrogen peroxide, iron ions, and manganese ions in the particle phase. The sources of OH radicals are one of the major uncertainties in SOA formation (Ervens et al., 2014).

The calculated  $\gamma$  and  $k_{\text{eff,uptake}}$  values for different seasons are listed in Table 3. The reactive uptake coefficients of glyoxal were in the range  $10^{-4}$ – $10^{-2}$ , and the average value of  $8.0 \times 10^{-3}$  in this study was close to the ones representing the loss of glyoxal by surface uptake during the KORUS-AQ campaign in a very recent study (Kim et al., 2022). The value slightly exceeded the one commonly used in model simulations ( $\gamma = 2.9 \times 10^{-3}$ ), which was based on an experimental study for  $(\text{NH}_4)_2\text{SO}_4$  aerosols at 55 % RH (Liggio et al., 2005a), and also far outweighs the uptake coefficients of glyoxal on clean and acidic gas-aged mineral particles ( $\gamma = 10^{-6}$ – $10^{-4}$ ) (Shen et al., 2016), implying that a real atmospheric aerosol provides a far more reactive interface for physiochemical processes than that of mineral particles. Moreover, uptake coefficients for methylglyoxal were with an average value of  $2.0 \times 10^{-3}$  and were higher than those reported in other experimental studies, which varied from  $10^{-6}$  to  $10^{-3}$  (Curry et al., 2018; De Haan et al., 2018). On the one hand, conflicting with previous experimental results (Waxman et al., 2015), methylglyoxal exhibited an unexpected salting-in effect in the real atmosphere due to much more complex compositions and higher ionic strength in ambient particles, which was also reported in other observational studies (Shen et al., 2018; Cui et al., 2021). The higher Henry's law coefficient values in Eq. (4) could lead to higher uptake coefficient values. On the other hand, a recent study

also provided direct experimental evidence to confirm that methylglyoxal is more reactive and has larger uptake coefficients on seed particles in atmospherically relevant concentrations (Li et al., 2021). The  $\gamma$  values for both glyoxal and methylglyoxal exhibited similar seasonal variations, which were lowest in summer and reached their highest in winter. This seasonal variation could be attributed to RH variation and particle composition. Moreover, the effective uptake rate ( $k_{\text{eff,uptake}}$ ), which is regarded as a pseudo-first-order reaction rate, is a net result of competition between reversible and irreversible processes, and it varied from  $10^{-4}$  to  $10^{-5} \text{ s}^{-1}$  in the real atmosphere in this study. As shown in Fig. 3a, the negative dependence of  $k_{\text{eff,uptake}}$  on RH also confirmed that the irreversible uptake of dicarbonyls could be inhibited in high RH conditions. What is more, as we can see in Fig. 3b, the irreversible uptake increased exponentially with increasing SNA (SNA: sulfate, nitrate, and ammonia) concentrations mainly because higher SNA concentrations always occurred in lower RH conditions with lower aerosol liquid water content (Fig. S8 in the Supplement), and the irreversible uptake was promoted by combined efforts of RH effects and ion effects, whereas, for a given RH, the uptake coefficient  $\gamma$  for both glyoxal and methylglyoxal showed a weak dependence on the ratio of SNA with significant scatter (Fig. S9 in the Supplement).

Moreover, it is worth noting that under extremely low RH ( $< 40\%$ ), the aerosol was not completely deliquescent, and the uptake coefficients based on Henry's law could not explain the irreversible pathways. Previous research indicated that the irreversible uptake of dicarbonyls could still occur under low RH conditions (Liggio et al., 2005a; De Haan et al., 2018) and that these uptake values were generally lower due to the inefficient reactive uptake process onto the crystallized aerosols.

#### 3.3.2 Reactive uptake of dicarbonyl compounds

We could not directly measure the particulate concentration of dicarbonyls via an irreversible pathway as the dicarbonyls irreversibly reacted with oxidative radicals on aerosols. To quantitatively evaluate the contribution of the irreversible pathway of dicarbonyls, we calculated their average concentration based on Eqs. (S3)–(S7) in the Supplement with the calculated  $\gamma$  values in this study. The samples estimated here were collected under high RH conditions (RH  $> 40\%$ ) because of the calculation limitation of irreversible uptake coefficients. Although the products of irreversible pathways could not be directly detected in particle phase and did not directly contribute to the increase in particulate dicarbonyls, the irreversible pathways could contribute to the decrease in gaseous dicarbonyls and explain well the overestimation of modelled dicarbonyl mixing ratios, which are about 3–6 times higher than the observed ones (Volkamer et al., 2007; Ling et al., 2020).

**Table 3.** Summary of calculated uptake coefficient  $\gamma$  and effective uptake rate coefficient  $k_{\text{eff,uptake}}$  in different seasons for glyoxal and methylglyoxal.

Dicarbonyl	Season	$T$ (K)	RH (%)	$\gamma$ ( $\times 10^{-3}$ )			$k_{\text{eff,uptake}}$ ( $\text{s}^{-1}$ ) ( $\times 10^{-4}$ )
				Average	Min	Max	
Glyoxal	Summer	301.1	67.7	4.15	0.12	7.30	1.61
	Autumn	287.2	45.4	8.62	0.29	12.9	4.83
	Spring	289.4	54.0	11.7	1.24	14.9	6.85
	Winter	273.5	54.0	10.6	0.56	14.4	3.59
	General*	287.8	59.0	8.0	0.46	11.4	3.38
Methylglyoxal	Summer	301.1	67.7	1.01	0.02	2.09	0.25
	Autumn	287.2	45.4	1.83	0.04	3.94	0.92
	Spring	289.4	54.0	2.36	0.06	4.34	0.69
	Winter	273.5	54.0	3.45	0.11	5.83	0.77
	General*	287.8	59.0	2.0	0.05	3.8	0.55

\* General is the average value of all the samples observed in the five field observations.

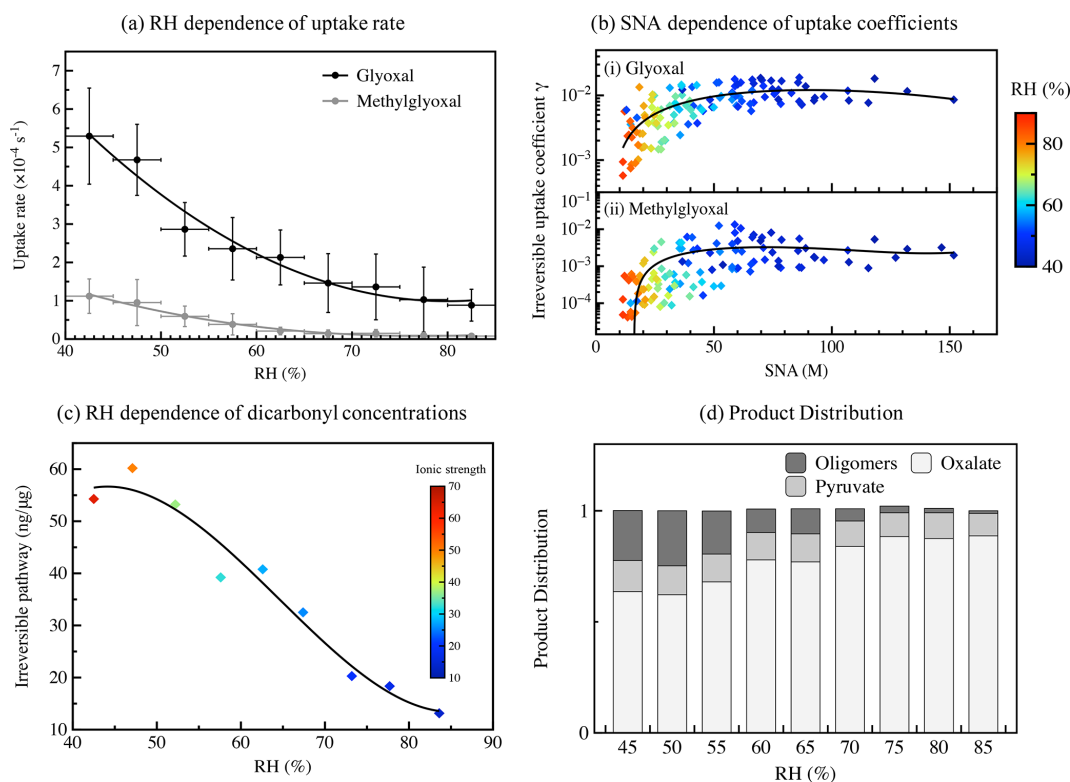


**Figure 3.** Gas–particle partitioning of dicarbonyls via irreversible pathways. **(a)** The RH dependence of irreversible uptake rate for glyoxal and methylglyoxal. **(b)** The SNA dependence of uptake coefficients for (i) glyoxal and (ii) methylglyoxal; SNA refers to the concentration of sulfate, nitrate, and ammonia in wet aerosols. **(c)** The RH dependence of particulate concentrations of dicarbonyl via irreversible pathways. **(d)** The corresponding modelled product distribution in wet aerosols under different RH conditions.

The total particulate concentration of glyoxal and methylglyoxal via irreversible pathways varied from several to more than 100 nanograms per microgram  $\text{PM}_{2.5}$  ( $\text{ng } \mu\text{g}^{-1} \text{PM}_{2.5}$ ), and it was strongly dependent on RH, as shown in Fig. 3c, which generally decreased with increasing RH. Concentrated

inorganic solutions and relatively higher ionic strength in aerosol water under low RH conditions could jointly contribute to the hydration of dicarbonyls, the products of which could easily participate into the following irreversible radical reactions via H abstraction.

To further discuss the product distribution of the reaction of glyoxal/methylglyoxal with hydroxyl radicals, we used the kinetic mechanisms of glyoxal/methylglyoxal + OH chemistry proposed by Lim et al. (2013) on the basis of a 0-D box model with a steady-state approach. The average OH radical concentration setting in the modelling was  $3.2 \times 10^{-12}$  M, which is based on the hypothesis of the Henry equilibrium of OH radicals between the gas and particle phases (Sander, 2015; Shen et al., 2018). Oxalate can be considered as a tracer for this aqueous chemistry since it does not have any other significant chemical sources. Oxalate was detected in the particle-phase samples by ion chromatography. The modelling results of oxalate concentration agreed well with the measured values, and their deviations were in the considered range (Fig. S10 in the Supplement). Meanwhile, we can estimate the distribution of major products in irreversible glyoxal/methylglyoxal + OH radical chemistry under different RH conditions, as illustrated in Fig. 3d. Generally, oxalate is the major product in wet aerosols, contributing  $\sim 60\%$ , and its proportion increases with increasing RH. Besides oxalate, oligomers also play significant roles in glyoxal/methylglyoxal + OH radical chemistry with a contribution of  $\sim 30\%$ , and their proportion is maximum under relatively low RH conditions. The RH dependence of the product distribution could mainly be attributed to the particulate concentration of glyoxal/methylglyoxal, which significantly affects the OH radical chemistry. With relatively high carbonyl concentrations (0.1–10 M) in aerosol liquid water, self-reactions of organic molecules become more favourable, resulting in new carbon–carbon bonds and high molecular weight oligomers via radical–radical chemistry (Lim et al., 2013). Moreover, besides OH radical chemistry, reaction with sulfate and ammonium also contributes to the oligomer formation and irreversible uptake of gaseous dicarbonyls (Ortiz-Montalvo et al., 2014; Lin et al., 2015; Lim et al., 2016). The oligomer proportion could be more than 30% in concentrated carbonyl solutions ( $\sim 0.1$  M) and only account for 1% in diluted solutions ( $\sim 0.01$  M).

### 3.4 Relative importance of two partitioning pathways

Table 4 summarizes the particulate concentration of glyoxal and methylglyoxal via reversible and irreversible pathways in different seasons. The average particulate concentrations of glyoxal ( $0.43 \text{ ng } \mu\text{g}^{-1}$  in the reversible pathway and  $24.26 \text{ ng } \mu\text{g}^{-1}$  in the irreversible pathway) were generally higher than those of methylglyoxal ( $0.25 \text{ ng } \mu\text{g}^{-1}$  in the reversible pathway and  $16.53 \text{ ng } \mu\text{g}^{-1}$  in the irreversible pathway), mainly due to the relatively higher water solubility and reactivity of glyoxal. Comparing two gas–particle partitioning processes, the irreversible pathway played extremely dominant roles and generally accounted for 96.7% and 95.0% for glyoxal and methylglyoxal, respectively. The proportion of the irreversible pathway varied from 90% to 99.9% and reached its highest in summer for glyoxal

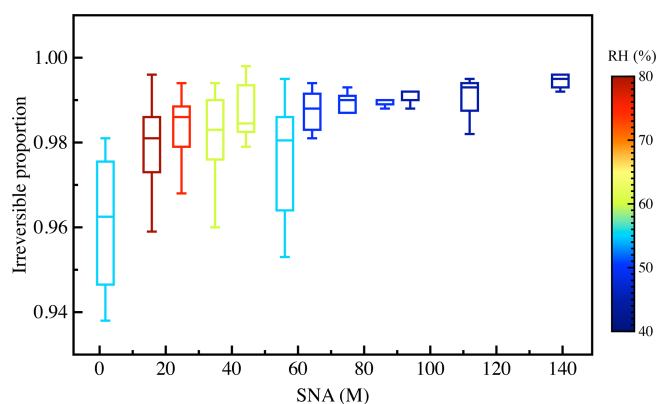


**Figure 4.** Correlation between the proportion of the irreversible pathway in the gas–particle partitioning process for dicarbonyls and aqueous sulfate, nitrate, and ammonia (SNA) concentrations in ambient aerosols under different relative humidity conditions.

(98.8%) and in autumn for methylglyoxal (99.2%), while it was minimum in winter (92.9% for glyoxal and 92.8% for methylglyoxal). Overall, the irreversible pathway played a dominant role in the gas–particle partitioning process for both glyoxal and methylglyoxal in the real atmosphere, while the reversible pathway was also substantial and non-negligible, especially in winter, with an proportion of  $\sim 10\%$ . Furthermore, as discussed above, the particulate concentrations of dicarbonyls and their relative importance were influenced by environmental factors such as relative humidity and particle composition, which could jointly influence both the reversible and irreversible pathways of dicarbonyls. As shown in Fig. 4, the proportion of irreversible pathways in the gas–particle partitioning process for dicarbonyls increased with aqueous SNA concentrations and reached maximum when SNA concentrations were more than 100 M under low RH conditions. Moreover, higher organic concentrations in aerosol may lead to an OH-limit environment, hindering the irreversible pathways driven by radicals and influencing the relative importance of the two pathways (Waxman et al., 2013; Ervens et al., 2014). But the OH limitations are still inclusive due to the uncertainties in the sources of OH in aerosol particles (Herrmann et al., 2010).

Comprehensively considering the contribution of both reversible pathways and irreversible pathways occurring in gas–particle partitioning processes could benefit the ambient dicarbonyl simulations. Ling et al. (2020) found that the observation and simulation of the gas-phase concentration level of dicarbonyls could reach reasonable agreement when the irreversible uptake and reversible partitioning were incorporated into the model as these jointly contribute  $\sim 62\%$  to the sink of dicarbonyls. Moreover, the contribution of gas–particle partitioning processes of dicarbonyls to SOA formation was higher as the two partitioning pathways were jointly considered. In this study, gas–particle partitioning processes of dicarbonyls accounted for a relatively large proportion

**Table 4.** Calculated relative importance of reversible and irreversible pathways in the gas–particle partitioning processes and their contribution to the particulate matter.

Season	Glyoxal		Methylglyoxal		Contribution to particulate matters
	[X] <sub>P,rever</sub> <sup>a</sup>	[X] <sub>P,irrever</sub> <sup>b</sup>	[X] <sub>P,rever</sub> <sup>a</sup>	[X] <sub>P,irrever</sub> <sup>b</sup>	
Summer	0.17 (1.2 %)	18.87 (98.8 %)	0.25 (5.5 %)	20.55 (94.5 %)	3.98 %
Autumn	0.14 (0.7 %)	23.91 (99.3 %)	0.12 (0.8 %)	17.02 (99.2 %)	4.12 %
Spring	0.26 (1.9 %)	15.94 (98.1 %)	0.09 (1.5 %)	14.16 (98.5 %)	3.05 %
Winter	0.89 (7.1 %)	34.70 (92.9 %)	0.38 (7.2 %)	12.59 (92.8 %)	4.86 %
General <sup>c</sup>	0.43 (3.3 %)	24.26 (96.7 %)	0.25 (5.0 %)	16.53 (95.0 %)	4.15 %

<sup>a</sup> [X]<sub>P,rever</sub> is the concentration of particle-phase carbonyl via reversible pathway (ng μg<sup>-1</sup>) and its proportion (%). <sup>b</sup> [X]<sub>P,irrever</sub> is the concentration of particle-phase carbonyl via irreversible pathways (ng μg<sup>-1</sup>) and its proportion (%). <sup>c</sup> General is the average value of all the samples observed in the five field observations.

of total particle mass (PM<sub>2.5</sub>), on average ~ 5 % considering both reversible and irreversible gas–particle partitioning pathways. Since a large fraction of PM<sub>2.5</sub> mass in Beijing consists of SOAs (~ 30 %) (Huang et al., 2014), we could roughly estimate the contribution of gas–particle partitioning processes of dicarbonyls to SOA yields (by mass). There were approximately 25 % SOAs formed from glyoxal and methylglyoxal in this study. However, the particulate dicarbonyls calculated here only contained simple reversible pathways and irreversible pathways driven by OH radicals. More complicated chemical processes, such as NO<sub>3</sub> radical chemistry, were not considered, which still resulted in the underestimation of their contribution to SOA formation.

#### 4 Conclusions

We simultaneously measured glyoxal and methylglyoxal concentrations in the gas and particle phases in different seasons over urban Beijing. Based on field-measured data, the field-derived gas–particle partitioning coefficients were calculated and found to be 5–7 magnitudes higher than the theoretical values. Such a large discrepancy provides field evidence that the gas–particle partitioning process does not occur by physical absorption alone but also results from the combined and simultaneous effects of reversible and irreversible pathways. Hydration and oligomerization occurred in the reversible pathway, producing compounds with lower volatility in the condensed phase, and the irreversible pathway could accelerate the uptake of gaseous dicarbonyls. The two pathways jointly contributed to the underestimation of gas–particle partitioning of dicarbonyls.

This study systemically considers both reversible and irreversible pathways in the ambient atmosphere for the first time. Compared to the reversible pathways, the irreversible pathways play a dominant role in the gas–particle partitioning process for dicarbonyls, accounting for ~ 90 % of this process. We recommend the irreversible reactive uptake coefficient for glyoxal and methylglyoxal in different seasons in the real atmosphere. The values we calculated here are higher

than those used in model simulations to date, especially for methylglyoxal which exhibits an unexpected salting-in effect under an atmospheric-relevant concentration. We expect the application of these parameterizations will increase the calculated contribution of irreversible uptake of dicarbonyls to SOA formation and narrow the gap between model predictions and field measurements of ambient dicarbonyl concentrations. Moreover, relative humidity and inorganic particle compositions are defined as the most important factor influencing particulate concentration and product distribution of dicarbonyls via both reversible and irreversible pathways, implying the significance of considering different RH conditions in dicarbonyl SOA simulations.

Furthermore, we note that there may be other potential explanations for the increase in particle mass caused by dicarbonyls and the uncertainty in the gas–particle partitioning process, including physical adsorption, reversible pathways, and irreversible pathways. Physical adsorption of dicarbonyls could be enhanced by water-soluble organics and mineral dust. Other reversible pathways, such as adducts formed from glyoxal with inorganic species, could also promote the gas–particle partitioning process. Irreversible pathways driven by other oxidants, such as NO<sub>3</sub> radicals, can also perform a substantial role. Shen et al. (2016) found that glyoxal could irreversibly produce formic acid, glycolic acid, and oligomers on particles without illumination or extra oxidants. Besides gas–particle partitioning, particulate dicarbonyls formed via the heterogeneous reaction of VOCs could contribute to the uncertainty in partitioning research. Dong et al. (2021) recently revealed that aqueous photo-oxidation of toluene could yield glyoxal and methylglyoxal via a ring-cleavage process. Overall, the real gas–particle partitioning process of glyoxal and methylglyoxal is more complicated, and their contribution to SOA formation is still indistinct; thus, more laboratory experiments and field measurements are urgently needed to improve our understanding of the gas–particle partitioning process for glyoxal and methylglyoxal.

**Data availability.** The data are accessible by contacting the corresponding author (zmchen@pku.edu.cn).

**Supplement.** The supplement related to this article is available online at: <https://doi.org/10.5194/acp-22-6971-2022-supplement>.

**Author contributions.** In the framework of the five field measurements in different seasons, ZC and JH designed the study, and JH performed all carbonyl measurements used in this study, analysed the data, and wrote the paper. ZC helped interpret the results, guided the writing, and modified the manuscript. XQ and PD contributed to the methods of sampling and analysing gas- and particle-phase carbonyls. All authors discussed the results and contributed to the final paper.

**Competing interests.** The contact author has declared that neither they nor their co-authors have any competing interests.

**Disclaimer.** Publisher's note: Copernicus Publications remains neutral with regard to jurisdictional claims in published maps and institutional affiliations.

**Acknowledgements.** We thank Shiyi Chen at Peking University for providing the data for the meteorological parameters, trace gases, and PM<sub>2.5</sub> mass concentrations.

**Financial support.** This research has been supported by the National Natural Science Foundation of China (grant no. 41975163).

**Review statement.** This paper was edited by Ivan Kourtev and reviewed by four anonymous referees.

## References

- Axson, J. L., Takahashi, K., De Haan, D. O., and Vaida, V.: Gas-phase water-mediated equilibrium between methylglyoxal and its geminal diol, *P. Natl. Acad. Sci. USA*, 107, 6687–6692, <https://doi.org/10.1073/pnas.0912121107>, 2010.
- Chen, X., Zhang, Y., Zhao, J., Liu, Y., Shen, C., Wu, L., Wang, X., Fan, Q., Zhou, S., and Hang, J.: Regional modeling of secondary organic aerosol formation over eastern China: The impact of uptake coefficients of dicarbonyls and semivolatile process of primary organic aerosol, *Sci. Total Environ.*, 793, 148176, <https://doi.org/10.1016/j.scitotenv.2021.148176>, 2021.
- Clegg, S. L., Brimblecombe, P., and Wexler, A. S.: Thermodynamic Model of the System  $\text{H}^+ - \text{NH}_4^+ - \text{SO}_4^{2-} - \text{NO}_3^- - \text{H}_2\text{O}$  at Tropospheric Temperatures, *J. Phys. Chem. A*, 102, 2137–2154, 1998.
- Cui, J., Sun, M., Wang, L., Guo, J., Xie, G., Zhang, J., and Zhang, R.: Gas-particle partitioning of carbonyls and its influencing factors in the urban atmosphere of Zhengzhou, China, *Sci. Total Environ.*, 751, 142027, <https://doi.org/10.1016/j.scitotenv.2020.142027>, 2021.
- Curry, L. A., Tsui, W. G., and McNeill, V. F.: Technical note: Updated parameterization of the reactive uptake of glyoxal and methylglyoxal by atmospheric aerosols and cloud droplets, *Atmos. Chem. Phys.*, 18, 9823–9830, <https://doi.org/10.5194/acp-18-9823-2018>, 2018.
- Davidovits, P., Kolb, C. E., Williams, L. R., Jayne, J. T., and Worsnop, D. R.: Mass Accommodation and Chemical Reactions at Gas-Liquid Interfaces, *Chem. Rev.*, 106, 1323–1354, <https://doi.org/10.1021/cr040366k>, 2006.
- De Haan, D. O., Jimenez, N. G., de Loera, A., Cazaunau, M., Gratién, A., Pangui, E., and Doussin, J. F.: Methylglyoxal Uptake Coefficients on Aqueous Aerosol Surfaces, *J. Phys. Chem. A*, 122, 4854–4860, <https://doi.org/10.1021/acs.jpca.8b00533>, 2018.
- Donaldson, D. J. and Vaida, V.: The Influence of Organic Films at the Air-Aqueous Boundary on Atmospheric Processes, *Chem. Rev.*, 106, 1445–1461, 2006.
- Dong, P., Chen, Z., Qin, X., and Gong, Y.: Water Significantly Changes the Ring-Cleavage Process During Aqueous Photooxidation of Toluene, *Environ. Sci. Technol.*, 55, 16316–16325, <https://doi.org/10.1021/acs.est.1c04770>, 2021.
- Elrod, M. J., Sedlak, J. A., and Ren, H.: Accurate Computational Model for the Hydration Extent of Atmospherically Relevant Carbonyls on Aqueous Atmospheric Particles, *ACS Earth and Space Chemistry*, 5, 348–355, <https://doi.org/10.1021/acsearthspacechem.0c00322>, 2021.
- Ervens, B. and Volkamer, R.: Glyoxal processing by aerosol multiphase chemistry: towards a kinetic modeling framework of secondary organic aerosol formation in aqueous particles, *Atmos. Chem. Phys.*, 10, 8219–8244, <https://doi.org/10.5194/acp-10-8219-2010>, 2010.
- Ervens, B., Sorooshian, A., Lim, Y. B., and Turpin, B. J.: Key parameters controlling OH-initiated formation of secondary organic aerosol in the aqueous phase (aqSOA), *J. Geophys. Res.-Atmos.*, 119, 3997–4016, <https://doi.org/10.1002/2013jd021021>, 2014.
- Faust, B. C. and Allen, J. M.: Aqueous-phase photochemical formation of hydroxyl radical in authentic cloudwaters and fogwaters, *Environ. Sci. Technol.*, 27, 113–122, 1993.
- Fu, T.-M., Jacob, D. J., Wittrock, F., Burrows, J. P., Vrekoussis, M., and Henze, D. K.: Global budgets of atmospheric glyoxal and methylglyoxal, and implications for formation of secondary organic aerosols, *J. Geophys. Res.*, 113, D15303, <https://doi.org/10.1029/2007jd009505>, 2008.
- Galloway, M. M., Chhabra, P. S., Chan, A. W. H., Surratt, J. D., Flagan, R. C., Seinfeld, J. H., and Keutsch, F. N.: Glyoxal uptake on ammonium sulphate seed aerosol: reaction products and reversibility of uptake under dark and irradiated conditions, *Atmos. Chem. Phys.*, 9, 3331–3345, <https://doi.org/10.5194/acp-9-3331-2009>, 2009.
- Guo, H., Xu, L., Bougiatioti, A., Cerully, K. M., Capps, S. L., Hite Jr., J. R., Carlton, A. G., Lee, S.-H., Bergin, M. H., Ng, N. L., Nenes, A., and Weber, R. J.: Fine-particle water and pH in the southeastern United States, *Atmos. Chem. Phys.*, 15, 5211–5228, <https://doi.org/10.5194/acp-15-5211-2015>, 2015.

- Haan, D. O. D., Corrigan, A. L., Smith, K. W., Stroik, D. R., Turley, J. J., Lee, F. E., Tolbert, M. A., Jimenez, J. L., Cordova, K. E., and Ferrell, G. R.: Secondary organic aerosol-forming reactions of glyoxal with amino acids, *Environ. Sci. Technol.*, 43, 2818, 2009.
- Hanson, D. R., Ravishankara, A. R., and Solomon, S.: Heterogeneous reactions in sulfuric acid aerosols: A framework for model calculations, *J. Geophys. Res.-Atmos.*, 99, 3615–3629, 1994.
- Hart, K. M. and Pankow, J. F.: High-Volume Air Sampler for Particle and Gas Sampling. 2. Use of Backup Filters To Correct for the Adsorption of Gas-Phase Polycyclic Aromatic Hydrocarbons to the Front Filter, *Environ. Sci. Technol.*, 28, 655–661, 1994.
- Hastings, W. P., Koehler, C. A., Bailey, E. L., and Haan, D. O. D.: Secondary organic aerosol formation by glyoxal hydration and oligomer formation: humidity effects and equilibrium shifts during analysis, *Environ. Sci. Technol.*, 39, 8728–8735, 2005.
- Healy, R. M., Wenger, J. C., Metzger, A., Duplissy, J., Kalberer, M., and Dommen, J.: Gas/particle partitioning of carbonyls in the photooxidation of isoprene and 1,3,5-trimethylbenzene, *Atmos. Chem. Phys.*, 8, 3215–3230, <https://doi.org/10.5194/acp-8-3215-2008>, 2008.
- Healy, R. M., Temime, B., Kuprovskite, K., and Wenger, J. C.: Effect of relative humidity on gas/particle partitioning and aerosol mass yield in the photooxidation of p-xylene, *Environ. Sci. Technol.*, 43, 1884–1889, 2009.
- Herrmann, H., Hoffmann, D., Schaefer, T., Brauer, P., and Tilgner, A.: Tropospheric aqueous-phase free-radical chemistry: radical sources, spectra, reaction kinetics and prediction tools, *Chemphyschem*, 11, 3796–3822, <https://doi.org/10.1002/cphc.201000533>, 2010.
- Hilal, S. H., Carreira, L. A., and Karickhoff, S. W.: Estimation of chemical reactivity parameters and physical properties of organic molecules using SPARC, in: *Quantitative Treatments of Solute/Solvent Interactions*, edited by: Murray, J. S., Elsevier, Amsterdam, the Netherlands, <http://ibmlc2.chem.uga.edu/sparc/index.cfm> (last access: 23 May 2021), 1994.
- Hu, J., Wang, P., Ying, Q., Zhang, H., Chen, J., Ge, X., Li, X., Jiang, J., Wang, S., Zhang, J., Zhao, Y., and Zhang, Y.: Modeling biogenic and anthropogenic secondary organic aerosol in China, *Atmos. Chem. Phys.*, 17, 77–92, <https://doi.org/10.5194/acp-17-77-2017>, 2017.
- Huang, R. J., Zhang, Y., Bozzetti, C., Ho, K. F., Cao, J. J., Han, Y., Daellenbach, K. R., Slowik, J. G., Platt, S. M., Canonaco, F., Zotter, P., Wolf, R., Pieber, S. M., Bruns, E. A., Crippa, M., Ciarelli, G., Piazzalunga, A., Schwikowski, M., Abbaszade, G., Schnelle-Kreis, J., Zimmermann, R., An, Z., Szidat, S., Baltensperger, U., El Haddad, I., and Prevot, A. S.: High secondary aerosol contribution to particulate pollution during haze events in China, *Nature*, 514, 218–222, <https://doi.org/10.1038/nature13774>, 2014.
- Ip, H., Huang, X., and Jian, Z. Y.: Effective Henry's law constants of glyoxal, glyoxylic acid, and glycolic acid, *Geophys. Res. Lett.*, 36, L01802, <https://doi.org/10.1029/2008GL036212>, 2009.
- Kampf, C. J., Waxman, E. M., Slowik, J. G., Dommen, J., Pfaffenberger, L., Praplan, A. P., Prevot, A. S., Baltensperger, U., Hoffmann, T., and Volkamer, R.: Effective Henry's law partitioning and the salting constant of glyoxal in aerosols containing sulfate, *Environ. Sci. Technol.*, 47, 4236–4244, <https://doi.org/10.1021/es400083d>, 2013.
- Kim, D., Cho, C., Jeong, S., Lee, S., Nault, B. A., Campuzano-Jost, P., Day, D. A., Schroder, J. C., Jimenez, J. L., Volkamer, R., Blake, D. R., Wisthaler, A., Fried, A., DiGangi, J. P., Diskin, G. S., Pusede, S. E., Hall, S. R., Ullmann, K., Huey, L. G., Tanner, D. J., Dibb, J., Knute, C. J., and Min, K.-E.: Field observational constraints on the controllers in glyoxal (CHOCHO) reactive uptake to aerosol, *Atmos. Chem. Phys.*, 22, 805–821, <https://doi.org/10.5194/acp-22-805-2022>, 2022.
- Kroll, J. H., Ng, N. L., Murphy, S. M., Varutbangkul, V., Flanagan, R. C., and Seinfeld, J. H.: Chamber studies of secondary organic aerosol growth by reactive uptake of simple carbonyl compounds, *J. Geophys. Res.*, 110, D23207, <https://doi.org/10.1029/2005jd006004>, 2005.
- Laskin, A., Laskin, J., and Nizkorodov, S. A.: Chemistry of atmospheric brown carbon, *Chem. Rev.*, 115, 4335–4382, <https://doi.org/10.1021/cr5006167>, 2015.
- Li, X., Rohrer, F., Brauers, T., Hofzumahaus, A., Lu, K., Shao, M., Zhang, Y. H., and Wahner, A.: Modeling of HCHO and CHOCHO at a semi-rural site in southern China during the PRIDE-PRD2006 campaign, *Atmos. Chem. Phys.*, 14, 12291–12305, <https://doi.org/10.5194/acp-14-12291-2014>, 2014.
- Li, Y., Ji, Y., Zhao, J., Wang, Y., Shi, Q., Peng, J., Wang, Y., Wang, C., Zhang, F., Wang, Y., Seinfeld, J. H., and Zhang, R.: Unexpected Oligomerization of Small alpha-Dicarbonyls for Secondary Organic Aerosol and Brown Carbon Formation, *Environ. Sci. Technol.*, 55, 4430–4439, <https://doi.org/10.1021/acs.est.0c08066>, 2021.
- Liggio, J.: Uptake of carbonyls to atmospheric particulate matter: Ambient measurements and laboratory studies, dissertation, York University, Canada, 2004.
- Liggio, J., Li, S. M., and McLaren, R.: Reactive uptake of glyoxal by particulate matter, *J. Geophys. Res.-Atmos.*, 110, D10304, <https://doi.org/10.1029/2004JD005113>, 2005a.
- Liggio, J., Shao-Meng, L. I., and McLaren, R.: Heterogeneous Reactions of Glyoxal on Particulate Matter: Identification of Acetals and Sulfate Esters, *Environ. Sci. Technol.*, 39, 1532–1541, 2005b.
- Lim, Y. B., Tan, Y., and Turpin, B. J.: Chemical insights, explicit chemistry, and yields of secondary organic aerosol from OH radical oxidation of methylglyoxal and glyoxal in the aqueous phase, *Atmos. Chem. Phys.*, 13, 8651–8667, <https://doi.org/10.5194/acp-13-8651-2013>, 2013.
- Lim, Y. B., Kim, H., Kim, J. Y., and Turpin, B. J.: Photochemical organonitrate formation in wet aerosols, *Atmos. Chem. Phys.*, 16, 12631–12647, <https://doi.org/10.5194/acp-16-12631-2016>, 2016.
- Lin, P., Laskin, J., Nizkorodov, S. A., and Laskin, A.: Revealing Brown Carbon Chromophores Produced in Reactions of Methylglyoxal with Ammonium Sulfate, *Environ. Sci. Technol.*, 49, 14257–14266, <https://doi.org/10.1021/acs.est.5b03608>, 2015.
- Ling, Z., Xie, Q., Shao, M., Wang, Z., Wang, T., Guo, H., and Wang, X.: Formation and sink of glyoxal and methylglyoxal in a polluted subtropical environment: observation-based photochemical analysis and impact evaluation, *Atmos. Chem. Phys.*, 20, 11451–11467, <https://doi.org/10.5194/acp-20-11451-2020>, 2020.
- Loeffler, K. W., Koehler, C. A., Paul, N. M., and Haan, D. D.: Oligomer formation in evaporating aqueous glyoxal and methyl glyoxal solutions, *Environ. Sci. Technol.*, 40, 6318, 2006.

- Lv, S., Gong, D., Ding, Y., Lin, Y., Wang, H., Ding, H., Wu, G., He, C., Zhou, L., Liu, S., Ristovski, Z., Chen, D., Shao, M., Zhang, Y., and Wang, B.: Elevated levels of glyoxal and methylglyoxal at a remote mountain site in southern China: Prompt in-situ formation combined with strong regional transport, *Sci. Total Environ.*, 672, 869–882, <https://doi.org/10.1016/j.scitotenv.2019.04.020>, 2019.
- Mader, B. T. and Pankow, J. F.: Gas/Solid Partitioning of Semivolatile Organic Compounds (SOCs) to Air Filters. 3. An Analysis of Gas Adsorption Artifacts in Measurements of Atmospheric SOC and Organic Carbon (OC) When Using Teflon Membrane Filters and Quartz Fiber Filters, *Environ. Sci. Technol.*, 35, 3422–3432, 2001.
- McNeill, V. F.: Aqueous organic chemistry in the atmosphere: sources and chemical processing of organic aerosols, *Environ. Sci. Technol.*, 49, 1237–1244, <https://doi.org/10.1021/es5043707>, 2015.
- Michailoudi, G., Lin, J. J., Yuzawa, H., Nagasaka, M., Huttula, M., Kosugi, N., Kurtén, T., Patanen, M., and Prisle, N. L.: Aqueous-phase behavior of glyoxal and methylglyoxal observed with carbon and oxygen K-edge X-ray absorption spectroscopy, *Atmos. Chem. Phys.*, 21, 2881–2894, <https://doi.org/10.5194/acp-21-2881-2021>, 2021.
- Mitsuishi, K., Iwasaki, M., Takeuchi, M., Okochi, H., Kato, S., Ohira, S.-I., and Toda, K.: Diurnal Variations in Partitioning of Atmospheric Glyoxal and Methylglyoxal between Gas and Particles at the Ground Level and in the Free Troposphere, *ACS Earth and Space Chemistry*, 2, 915–924, <https://doi.org/10.1021/acsearthspacechem.8b00037>, 2018.
- Odabasi, M. and Seyfioglu, R.: Phase partitioning of atmospheric formaldehyde in a suburban atmosphere, *Atmos. Environ.*, 39, 5149–5156, <https://doi.org/10.1016/j.atmosenv.2005.05.006>, 2005.
- Odum, J. R., Hoffmann, T., Bowman, F., Collins, D., Flagan, R. C., and Seinfeld, J. H.: Gas/Particle Partitioning and Secondary Organic Aerosol Yields, *Environ. Sci. Technol.*, 30, 2580–2585, 1996.
- Ortiz-Montalvo, D. L., Hakkinen, S. A., Schwieter, A. N., Lim, Y. B., McNeill, V. F., and Turpin, B. J.: Ammonium addition (and aerosol pH) has a dramatic impact on the volatility and yield of glyoxal secondary organic aerosol, *Environ. Sci. Technol.*, 48, 255–262, <https://doi.org/10.1021/es4035667>, 2014.
- Pankow, J. F.: An absorption model of GAS/Particle partitioning of organic compounds in the atmosphere, *Atmos. Environ.*, 28, 185–188, [https://doi.org/10.1016/1352-2310\(94\)90093-0](https://doi.org/10.1016/1352-2310(94)90093-0), 1994.
- Pankow, J. F. and James, F.: An absorption model of the gas/aerosol partitioning involved in the formation of secondary organic aerosol, *Atmos. Environ.*, 28, 189–193, 1994.
- Qian, X., Shen, H., and Chen, Z.: Characterizing summer and winter carbonyl compounds in Beijing atmosphere, *Atmos. Environ.*, 214, 116845, <https://doi.org/10.1016/j.atmosenv.2019.116845>, 2019.
- Qiu, X., Wang, S., Ying, Q., Duan, L., Xing, J., Cao, J., Wu, D., Li, X., Chengzhi, X., Yan, X., Liu, C., and Hao, J.: Importance of Wintertime Anthropogenic Glyoxal and Methylglyoxal Emissions in Beijing and Implications for Secondary Organic Aerosol Formation in Megacities, *Environ. Sci. Technol.*, 54, 11809–11817, <https://doi.org/10.1021/acs.est.0c02822>, 2020.
- Rao, Z., Chen, Z., Liang, H., Huang, L., and Huang, D.: Carbonyl compounds over urban Beijing: Concentrations on haze and non-haze days and effects on radical chemistry, *Atmos. Environ.*, 124, 207–216, <https://doi.org/10.1016/j.atmosenv.2015.06.050>, 2016.
- Sander, R.: Compilation of Henry's law constants (version 4.0) for water as solvent, *Atmos. Chem. Phys.*, 15, 4399–4981, <https://doi.org/10.5194/acp-15-4399-2015>, 2015.
- Sareen, N., Schwieter, A. N., Shapiro, E. L., Mitroo, D., and McNeill, V. F.: Secondary organic material formed by methylglyoxal in aqueous aerosol mimics, *Atmos. Chem. Phys.*, 10, 997–1016, <https://doi.org/10.5194/acp-10-997-2010>, 2010.
- Saxena, P. and Hildemann, L. M.: Water-soluble organics in atmospheric particles: A critical review of the literature and application of thermodynamics to identify candidate compounds, *J. Atmos. Chem.*, 24, 57–109, 1996.
- Schweitzer, F., Magi, L., Mirabel, P., and George, C.: Uptake Rate Measurements of Methanesulfonic Acid and Glyoxal by Aqueous Droplets, *J. Phys. Chem. A*, 102, 593–600, 1998.
- Schwieter, A. N., Sareen, N., Mitroo, D., Shapiro, E. L., and McNeill, V. F.: Glyoxal-methylglyoxal cross-reactions in secondary organic aerosol formation, *Environ. Sci. Technol.*, 44, 6174–6182, 2010.
- Shen, H., Chen, Z., Li, H., Qian, X., Qin, X., and Shi, W.: Gas-Particle Partitioning of Carbonyl Compounds in the Ambient Atmosphere, *Environ. Sci. Technol.*, 52, 10997–11006, <https://doi.org/10.1021/acs.est.8b01882>, 2018.
- Shen, X., Wu, H., Zhao, Y., Huang, D., Huang, L., and Chen, Z.: Heterogeneous reactions of glyoxal on mineral particles: A new avenue for oligomers and organosulfate formation, *Atmos. Environ.*, 131, 133–140, <https://doi.org/10.1016/j.atmosenv.2016.01.048>, 2016.
- Shi, Q., Zhang, W., Ji, Y., Wang, J., Qin, D., Chen, J., Gao, Y., Li, G., and An, T.: Enhanced uptake of glyoxal at the acidic nanoparticle interface: implications for secondary organic aerosol formation, *Environ. Sci.-Nano*, 7, 1126–1135, <https://doi.org/10.1039/d0en00016g>, 2020.
- Tan, Y., Lim, Y. B., Altieri, K. E., Seitzinger, S. P., and Turpin, B. J.: Mechanisms leading to oligomers and SOA through aqueous photooxidation: insights from OH radical oxidation of acetic acid and methylglyoxal, *Atmos. Chem. Phys.*, 12, 801–813, <https://doi.org/10.5194/acp-12-801-2012>, 2012.
- Teich, M., Pinxteren, D. V., Kecorius, S., Wang, Z., and Herrmann, H.: First Quantification of Imidazoles in Ambient Aerosol Particles: Potential Photosensitizers, Brown Carbon Constituents, and Hazardous Components, *Environ. Sci. Technol.*, 50, 1166–1173, 2016.
- Volkamer, R., San Martini, F., Molina, L. T., Salcedo, D., Jimenez, J. L., and Molina, M. J.: A missing sink for gas-phase glyoxal in Mexico City: Formation of secondary organic aerosol, *Geophys. Res. Lett.*, 34, L19807, <https://doi.org/10.1029/2007gl030752>, 2007.
- Wang, H., Zhang, X., and Chen, Z.: Development of DNPH/HPLC method for the measurement of carbonyl compounds in the aqueous phase: applications to laboratory simulation and field measurement, *Environ. Chem.*, 6, <https://doi.org/10.1071/en09057>, 2009.
- Waxman, E. M., Dzepina, K., Ervens, B., Lee-Taylor, J., Aumont, B., Jimenez, J. L., Madronich, S., and Volkamer, R.: Secondary organic aerosol formation from semi- and intermediate-volatility

- organic compounds and glyoxal: Relevance of O/C as a tracer for aqueous multiphase chemistry, *Geophys. Res. Lett.*, 40, 978–982, <https://doi.org/10.1002/grl.50203>, 2013.
- Waxman, E. M., Elm, J., Kurten, T., Mikkelsen, K. V., Ziemann, P. J., and Volkamer, R.: Glyoxal and Methylglyoxal Setschenow Salting Constants in Sulfate, Nitrate, and Chloride Solutions: Measurements and Gibbs Energies, *Environ. Sci. Technol.*, 49, 11500–11508, <https://doi.org/10.1021/acs.est.5b02782>, 2015.
- Williams, B. J., Goldstein, A. H., Kreisberg, N. M., and Hering, S. V.: In situ measurements of gas/particle-phase transitions for atmospheric semivolatile organic compounds, *P. Natl. Acad. Sci. USA*, 107, 6676–6681, <https://doi.org/10.1073/pnas.0911858107>, 2010.
- Xie, M., Hannigan, M. P., and Barsanti, K. C.: Gas/particle partitioning of 2-methyltetrols and levoglucosan at an urban site in Denver, *Environ. Sci. Technol.*, 48, 2835–2842, <https://doi.org/10.1021/es405356n>, 2014.
- Xu, R., Li, X., Dong, H., Wu, Z., Chen, S., Fang, X., Gao, J., Guo, S., Hu, M., Li, D., Liu, Y., Liu, Y., Lou, S., Lu, K., Meng, X., Wang, H., Zeng, L., Zong, T., Hu, J., Chen, M., Shao, M., and Zhang, Y.: Measurement of gaseous and particulate formaldehyde in the Yangtze River Delta, China, *Atmos. Environ.*, 224, 117114, <https://doi.org/10.1016/j.atmosenv.2019.117114>, 2020.
- Ying, Q., Li, J., and Kota, S. H.: Significant Contributions of Isoprene to Summertime Secondary Organic Aerosol in Eastern United States, *Environ. Sci. Technol.*, 49, 7834–7842, <https://doi.org/10.1021/acs.est.5b02514>, 2015.
- Zarzana, K. J., Min, K. E., Washenfelder, R. A., Kaiser, J., Krawiec-Thayer, M., Peischl, J., Neuman, J. A., Nowak, J. B., Wagner, N. L., Dube, W. P., St Clair, J. M., Wolfe, G. M., Hanisco, T. F., Keutsch, F. N., Ryerson, T. B., and Brown, S. S.: Emissions of Glyoxal and Other Carbonyl Compounds from Agricultural Biomass Burning Plumes Sampled by Aircraft, *Environ. Sci. Technol.*, 51, 11761–11770, <https://doi.org/10.1021/acs.est.7b03517>, 2017.
- Zarzana, K. J., Selimovic, V., Koss, A. R., Sekimoto, K., Coggon, M. M., Yuan, B., Dubé, W. P., Yokelson, R. J., Warneke, C., de Gouw, J. A., Roberts, J. M., and Brown, S. S.: Primary emissions of glyoxal and methylglyoxal from laboratory measurements of open biomass burning, *Atmos. Chem. Phys.*, 18, 15451–15470, <https://doi.org/10.5194/acp-18-15451-2018>, 2018.
- Zhao, J., Levitt, N. P., Zhang, R., and Chen, J.: Heterogeneous reactions of methylglyoxal in acidic media: implications for secondary organic aerosol formation, *Environ. Sci. Technol.*, 40, 7682–7687, 2006.
- Zhu, Y., Yang, L., Chen, J., Kawamura, K., Sato, M., Tilgner, A., van Pinxteren, D., Chen, Y., Xue, L., Wang, X., Simpson, I. J., Herrmann, H., Blake, D. R., and Wang, W.: Molecular distributions of dicarboxylic acids, oxocarboxylic acids and  $\alpha$ -dicarbonyls in PM<sub>2.5</sub> collected at the top of Mt. Tai, North China, during the wheat burning season of 2014, *Atmos. Chem. Phys.*, 18, 10741–10758, <https://doi.org/10.5194/acp-18-10741-2018>, 2018.